

## EFFECTS OF TEMPERATURE ON ELASTIC STIFFNESS OF A HDPE GEOGRID AND ITS MODEL SIMULATION

Thitapan Chantachot<sup>1</sup>, \*Warat Kongkitkul<sup>2</sup> and Fumio Tatsuoka<sup>3</sup>

<sup>1,2</sup>Department of Civil Engineering, Faculty of Engineering,  
King Mongkut's University of Technology Thonburi, Thailand

<sup>3</sup>Department of Civil Engineering, Tokyo University of Science, Japan

\*Corresponding Author, Received: 18 June 2016, Revised: 15 July 2016, Accepted: 26 Nov. 2016

**ABSTRACT:** One of the important factors that affect the mechanical properties of polymer geosynthetic reinforcement is the ambient temperature. With an increase in the temperature, the rupture strength and the elastic stiffness decrease. In this study, to understand the temperature effects on the load-strain-time behaviours of a polymer geogrid, a series of tensile loading tests were performed on a high-density polyethylene (HDPE) geogrid at different but constant temperatures, and also under step-increasing temperature conditions. The test results revealed that the elastic stiffness of tested geogrid increases with the load level, while decreases with the ambient temperature. These properties were modelled based on the framework of hypo-elasticity. An existing non-linear three-component (NTC) model, which can simulate the load-strain-time behaviours of many types of polymer geogrid subjected to arbitrary loading histories (e.g., monotonic loading at different rates, creep or sustained loading, load relaxation) under a constant temperature, was modified to account for the dependency of the elastic stiffness on the load level and the temperature, as well as the dependency of the rupture strength on the temperature. The modified model can simulate very well the observed temperature effects on the elasticity of the tested geogrid.

*Keywords: Elastic Stiffness, Geogrid, Non-Linear Three-Component Model, Temperature*

### 1. INTRODUCTION

A number of different types of polymer geosynthetic reinforcement are used as reinforcements for various geotechnical engineering structures (e.g., slopes, embankments, and retaining walls). Typically, constructions of these structures utilising geosynthetic reinforcements are faster and more cost-effective than ordinary conventional methods. In design of a geosynthetic-reinforced soil (GRS) structure, it is required to know the mechanical properties of a given geosynthetic reinforcement, especially the rupture tensile strength. However, it is usually determined for an ambient temperature condition that is controlled constant throughout a test (equal to 20 °C following ASTM D4595 [1] and EN ISO 10319 [2]).

On the other hand, air-temperature cyclically changes both daily and seasonally. This variation of air-temperature affects the ambient temperature of backfill in a GRS structure, and thereafter, the geosynthetic reinforcements arranged inside [3]. From field monitoring of a GRS structure, changes of air-temperature were found to correlate with the geogrid strains arranged inside [3]-[4]. Moreover, effects of temperature rise on the load-strain-time behaviours of geosynthetic reinforcements were also studied in the laboratory [5]-[9]. It was found that not only the rupture strength but also the pre-peak stiffness and the elastic stiffness decrease with an increase in the temperature. Therefore, the study of

temperature effects on the load-strain-time behaviours of geosynthetic reinforcements is of a great importance.

To simulate the rate-dependent behaviours of geosynthetic reinforcements (i.e., monotonic loading at different but constant strain rates, creep or sustained loading, and load relaxation), an elasto-viscoplastic non-linear three-component (NTC) model was proposed [10]-[12]. Subsequently, the NTC model was modified to simulate temperature-accelerated creep tests by taking into account the effects of temperature increase on the rupture tensile strength and stiffness of geosynthetic reinforcement [13]. The simulation results indicated that the NTC model is capable of simulating both rate- and temperature-dependent behaviours. However, in this previous study, the elastic stiffness was treated unaffected by the temperature rise, and validation of the model with experimental data has not been performed.

In view of the above, in this study, a series of tensile loading tests were performed to evaluate effects of temperature and load/temperature history on the elastic stiffness of a HDPE geogrid. Then, the NTC model was modified to realistically simulate the test results by incorporating the dependency of the elastic stiffness on the temperature.

## 2. ELASTIC STIFFNESS AS A FUNCTION OF LOAD LEVEL AND TEMPERATURE

To determine the elastic stiffness,  $k_{eq}$ , of a geosynthetic reinforcement, small-amplitude unload-reload cyclic loading tests have been performed on many types of geogrid [7]. Then, the following formulations of dependency of  $k_{eq}$  on the load level and the temperature was proposed:

$$k_{eq} = k_{eq0}(T) \left( \frac{V}{V_{max}} \right)^m \quad (1)$$

$$k_{eq0} = p'(A^{f'})^{q'} \quad (2)$$

where:  $k_{eq0}(T)$  is the value of  $k_{eq}$  when  $V/V_{max} = 1$ ;  $V/V_{max}$  is the load level, defined as the ratio of the tensile load,  $V$ , to the maximum tensile load at respective ambient temperature,  $V_{max}$ ;  $m$ ,  $p'$  and  $q'$  are the material constants, depending on types of polymer geosynthetic reinforcement; and  $A^{f'}$  is the temperature effect parameter, defined as the ratio of the rupture strength at a given temperature to the rupture strength at standard temperature of 20 °C [1], [2]. Note that rupture tensile strength is defined for the strain rate at rupture equal to 0.1 %/min.

## 3. TEST MATERIAL AND PROGRAMME

In this study, to determine the elastic stiffness and the temperature effect parameter, a series of special tensile loading tests were performed on a high-density polyethylene (HDPE) geogrid, employing the following two different loading patterns: i) continuous monotonic loading (ML) until the rupture; and ii) sustained (creep) loading (SL) applied during otherwise ML until rupture. A constant load rate of 0.6 kN/m/min was used for ML in both loading patterns i) and ii). In loading pattern ii), ML was first performed until achieving the specified tensile load and then SL was held for three hours, after which another ML was restarted until the rupture. The ambient temperature surrounding the test specimen was controlled constant throughout a test at either 30, 40 or 50 °C by means of a temperature-controlled chamber [7].

## 4. TEST RESULTS AND DISCUSSIONS

### 4.1 Temperature Effect Parameter

The relationships between tensile load,  $V$ , and tensile strain,  $\epsilon$ , obtained from ML tests at different but constant temperatures are shown in Fig. 1. In these tests, any rupture was not observed at the ends

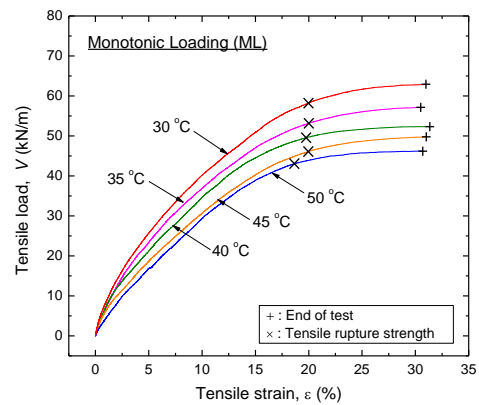


Fig. 1 Tensile load-tensile strain relations from continuous ML tests (loading pattern i) under different constant temperatures

Table 1 Rupture strengths under different constant temperatures

Temperature (°C)	Rupture strength (kN/m)
30	53.2
35	48.1
40	44.9
45	41.8
50	38.9

Note: rupture strength was defined for the strain rate at rupture equal to 0.1 %/min

of the test (denoted by symbol “+”), because of a limited maximum stroke of the tensile loading machine. Therefore, the rupture tensile strengths were defined at the points of maximum curvature along the respective  $V - \epsilon$  relations (denoted by symbol “x”). Then, these values were corrected to the values at the same strain rate (equal to 0.1 %/min) to eliminate the effects of strain rate on the tensile rupture strength of geosynthetic reinforcements [7]. The values of corrected rupture strength are summarised in Table 1. It can be seen that with the increasing temperature, the rupture strength decreases.

Figure 2 shows a relationship between the temperature effect parameter,  $A^{f'}$ , and the temperature,  $T$ . The value of  $A^{f'}$  is unity at the standard temperature,  $T'_0$ , of 20 °C. The procedures to determine the  $A^{f'}$  value are explained in details in Kongkitkul *et al.* [7]. It can be seen that the  $A^{f'}$  value decreases from unity at  $T'_0 = 20$  °C to a smaller value at a higher temperature. Thus the reduction of rupture tensile strength with the increasing temperature of HDPE geogrid can be described by Eq. (2), which incorporates  $A^{f'}$ .

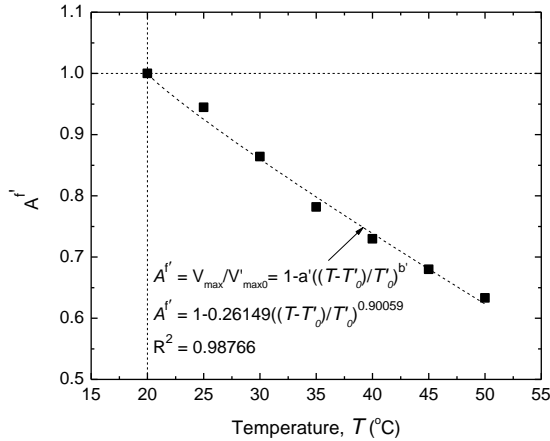


Fig. 2 Temperature effect parameter,  $A^{f'}$ , as a function of temperature,  $T$

## 4.2 Elastic Stiffness

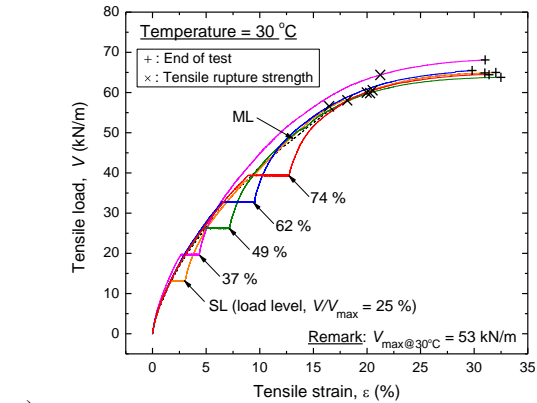
### 4.2.1 Determination of elastic stiffness

Figures 3(a) to 3(c) show the  $V - \epsilon$  relations of the HDPE geogrid by SL under different temperatures equal to 30, 40, and 50 °C, respectively. In these figures, SL tests were performed at different tensile load levels,  $V/V_{max}$ . The values of  $V_{max}$  at respective temperature are shown in Table 1. It can be seen that  $V - \epsilon$  relation of the geogrid exhibits a very high stiffness, close to the elastic value when ML was restarted following SL [9]. Therefore, in this study, the elastic stiffness was determined from a linear relation fitted to the initial  $V - \epsilon$  curve immediately after the restart of ML following SL, as shown in Fig. 4.

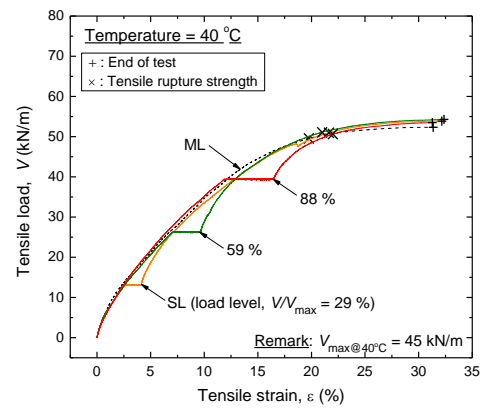
### 4.2.2 Effects of load level and temperature on elastic stiffness

Figure 5(a) shows the elastic stiffness,  $k_{eq}$ , versus the load level,  $V/V_{max}$ , relations in the full-log plot of HPDE geogrid for different temperatures. The lines fitted to the data points for respective temperatures represent Eq. (1). It is readily seen that  $k_{eq}$  increases significantly with an increase in the load level, while drastically decreases with an increase in the temperature. These behaviours indicate that the  $k_{eq}$  values of HDPE geogrid exhibit a combination of the hypo-elasticity and the degradation by temperature effects.

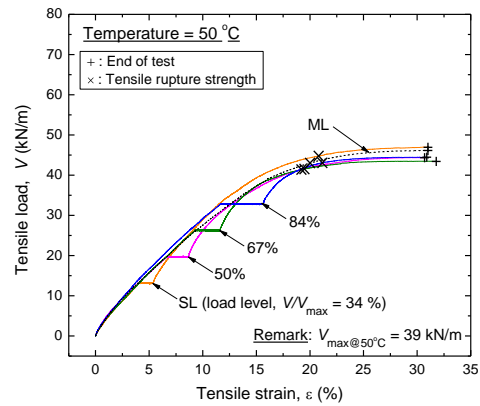
The behaviours of  $k_{eq}$  determined by the method used in the present study are similar to those reported by Kongkitkul *et al.* [7], in which the  $k_{eq}$  values of the same HPDE geogrid were determined by measuring the slope  $V - \epsilon$  relations during small-amplitude cyclic loadings. Equation (1) was



a)



b)



c)

Fig. 3 Tensile load-tensile strain relations from SL tests during otherwise ML (loading pattern ii) under different temperatures of: (a) 30 °C; (b) 40 °C; and (c) 50 °C

used to best fit to the  $k_{eq} - V/V_{max}$  data points obtained in this study (Fig. 5(a)). It can be seen that the lines fitted to the data points from the present study are agreed very well with the data points from Kongkitkul *et al.* [7]. In Fig. 5(b), the  $k_{eq0}$  values according to Eq. (1) obtained from the fitted relations shown in Fig. 5(a) were plotted against

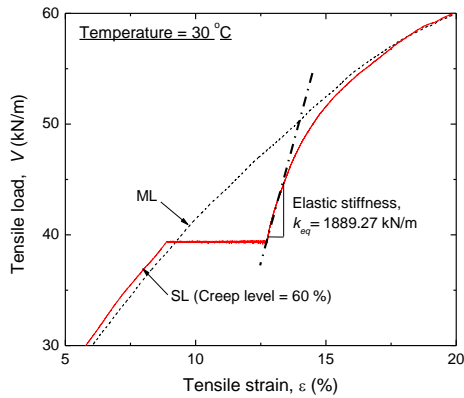


Fig. 4 Determination of elastic stiffness from  $V - \varepsilon$  relation immediately at the restart of ML following SL

the  $A^{f'}$  values for the respective temperatures obtained from Fig. 2. Then, Eq. (2) was fitted to the plotted  $k_{eq0}$  and  $A^{f'}$  data from the present study. It may be seen that the fitted curve is also in good agreement with the data points from Kongkitkul *et al.* [7].

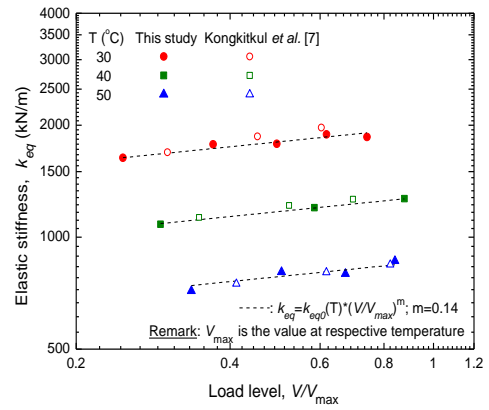
## 5. MODELLING OF ELASTIC PROPERTIES

### 5.1 Non-Linear Three-component Model

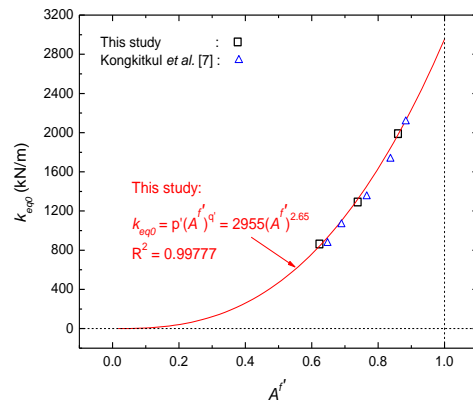
For realistic simulation of the load-strain-time behaviours of polymer geosynthetic reinforcements under a constant temperature, an elasto-viscoplastic non-linear three-component (NTC) model was developed [10]. This NTC model consists of elastic, inviscid, and viscous components. In the elastic component, elastic strain rate,  $\dot{\varepsilon}^e$ , is determined by an hypo-elastic model having the equivalent elastic modulus,  $k_{eq}(V)$ , that is a function of instantaneous tensile load,  $V$ :

$$\dot{\varepsilon}^e = \dot{V} / k_{eq}(V) \quad (3)$$

On the other hand, with an increase in the temperature,  $T$ , the  $k_{eq}(V)$  value at a given load level decreases (Fig. 5(a)). To take into account the coupled effects of load level,  $V/V_{max}$ , and temperature,  $T$ , on elastic stiffness,  $k_{eq}(V, T)$ , the NTC model was modified as follows. Figure 6 shows the method to obtain the current elastic stiffness from the current temperature,  $T$ , the current tensile load  $V$ , and a known rupture strength at  $T'_0 = 20$  °C,  $V'_{max0}$ . By implementing the algorithm shown in Fig. 6 into the modified NTC model, the realistic current elastic stiffness can be easily determined.



a)



b)

Fig. 5 Elastic stiffness as a function of load level and temperature: (a)  $k_{eq} - V/V_{max}$  relations; and (b)  $k_{eq0} - A^{f'}$  relation

### 5.2 Simulation Results

The  $V - \varepsilon$  relations from continuous ML tests at different constant temperatures are presented in Fig. 7(a), while those from tests in which SL was performed during otherwise ML (as those shown in Fig. 7(a)) are presented in Fig. 8 (a). Figures 7(a) and 8(a) compare these experimental results and their simulations. It can be seen that the modified NTC model can simulate very well the measured  $V - \varepsilon$  relations for various load/temperature histories. The dependency of  $k_{eq}$  on the load level and temperature can be seen very well from the tensile load,  $V$ , versus the elastic tensile strain,  $\varepsilon^e$ , relations shown in Figs. 7(b) and 8(b). The tangential slope of  $V - \varepsilon^e$  relation is equal to the current  $k_{eq}$  value. It can be seen from Fig. 7(b) that, at any given  $V$  value, the  $k_{eq}$  value decreases with an increase in the temperature. On the other hand, at the same temperature, the  $k_{eq}$  value increases with an increase in  $V$ . This result indicates that the modified NTC model can successfully simulate the coupled effects of load level and temperature on the elastic stiffness.

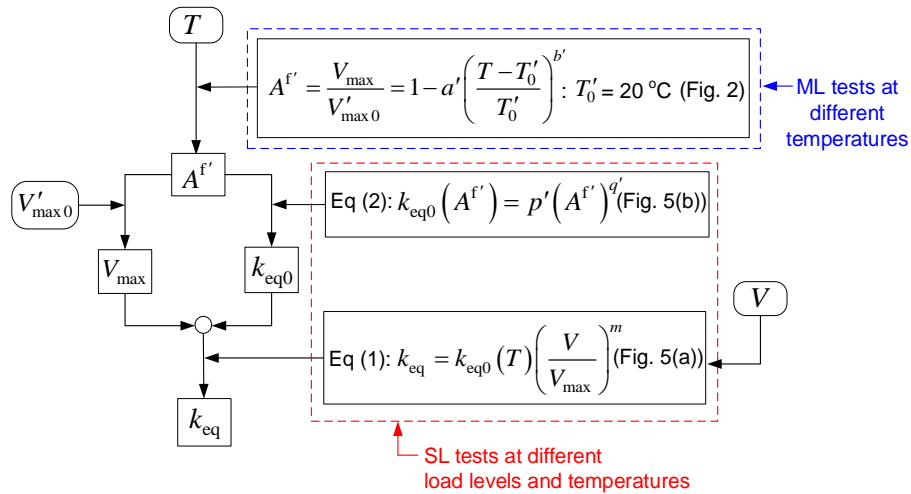


Fig. 6 Diagram to obtain the current elastic stiffness value (modified from Kongkitkul *et al.* [7])

The experimental and simulation results described above were obtained under the conditions of constant temperature. To further examine the capability of the modified NTC model, a series of tests in which the temperature was increased during SL from 30 °C at the start of SL to 50 °C at the end of SL was performed. Then, the results of these tests and their simulations are presented and compared in Fig. 8(a). Figure 8(b) compares the simulated  $V - \varepsilon^e$  relation for the SL test in which the temperature was increased from 30 °C to 50 °C during otherwise ML with the simulated  $V - \varepsilon^e$  relations in continuous ML tests during which a SL was performed at an intermediate load level under different constant temperatures of 30, 40, and 50 °C. It can be readily seen that the  $V - \varepsilon^e$  states during SL tests under either constant or varying temperature do not move as the tensile loads are kept constant. As a result, the entire  $V - \varepsilon^e$  relation from the origin to the end of an intermission of ML by SL under the constant temperature condition does not change, like that obtained by a continuous ML test at a constant temperature. On the other hand, upon the restart of continuous ML at an elevated temperature (i.e., 50 °C) after a SL test during which the temperature increases from 30 °C to 50 °C, the  $V - \varepsilon^e$  relation starts from a point along the  $V - \varepsilon^e$  relation from the continuous ML at a constant temperature of 30 °C while exhibiting a drastic decrease in the slope to the one of the  $V - \varepsilon^e$  relation from the continuous ML at a constant temperature of 50 °C, as shown in Fig. 8(c).

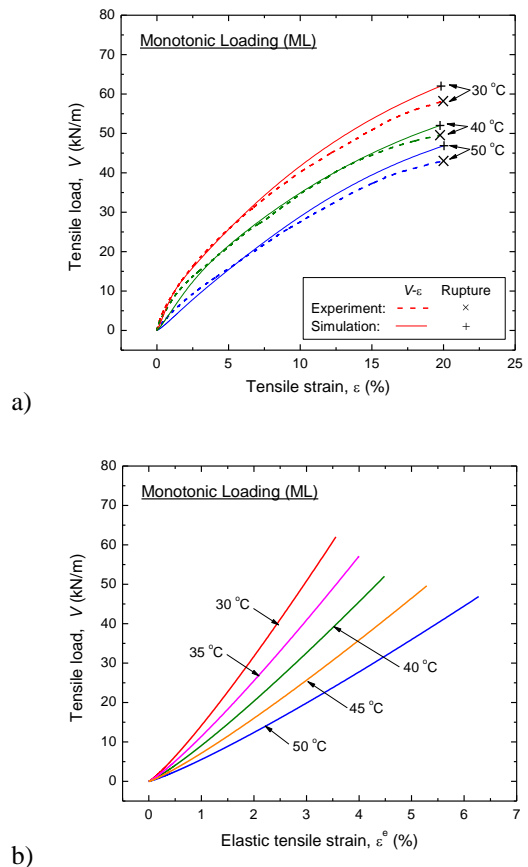


Fig. 7 Behaviours in continuous ML tests under different temperatures: (a) measured and simulated  $V - \varepsilon$  relations; and (b) simulated  $V - \varepsilon^e$  relations

## 6. CONCLUSIONS

The following conclusions can be derived from the experimental and simulation results that were observed in this study:

1. Rupture tensile strength of the tested HDPE geogrid decreases with an increase in the temperature.
2. Elastic stiffness increases with an increase in the load level, while decreases with an increase in the temperature. These trends of behaviour can be expressed by the coupled functional forms proposed in this study.
3. The modified NTC model can well-simulate the variation of elastic stiffness, as a result of the coupled effects between the load level and the temperature.

## 7. ACKNOWLEDGEMENTS

The authors would like to acknowledge the support from Department of Civil Engineering, King Mongkut's University of Technology Thonburi (CE-KMUTT-FTERO 5801). Thanks are also extended to Thailand Research Fund (TRF), Thailand. The HDPE geogrid used in this study was provided from Vigor Merger Co., Ltd.

## 8. REFERENCES

- [1] ASTM D4595-11, Standard Test Method for Tensile Properties of Geotextiles by the Wide-Width Strip Method, ASTM International, West Conshohocken, PA, USA, 2011.
- [2] EN ISO 10319:2008, Geosynthetics-Wide-Width Tensile Test, International Organization for Standardization, Geneva, Switzerland, 2008.
- [3] Fannin RJ, "Long-term variations of force and strain in a steep geogrid-reinforced soil slope", *Geosynthetics International*, Vol. 8, No. 1, Jan. 2001, pp. 81-96.
- [4] Tatsuoka F, Tateyama M, Koda M, Kojima K, Yonezawa T, Shindo Y, & Tamai S, "Research and construction of geosynthetic-reinforced soil integral bridges", *Transportation Geotechnics*, Vol. 8, Sep. 2016, pp. 4-25.
- [5] Zornberg JG, Byler BB, & Knudsen JW, "Creep of geotextiles using Time-Temperature Superposition methods", *J. of Geotechnical and Geoenvironmental Engineering*, Vol. 130, No. 11, Nov. 2004, pp. 1158-1168.
- [6] Hsieh C, and Tseng YC, "Tensile creep behavior of a PVC coated polyester geogrid at different temperatures", *J. of GeoEngineering*, Vol. 3, No. 3, Dec. 2008, pp. 113-119.
- [7] Kongkitkul W, Tabsombut W, Jaturapitakkul C, & Tatsuoka F, "Effects of temperature on the rupture strength and elastic stiffness of geogrids", *Geosynthetics International*, Vol. 19, No. 2, Apr. 2012, pp. 106-123.

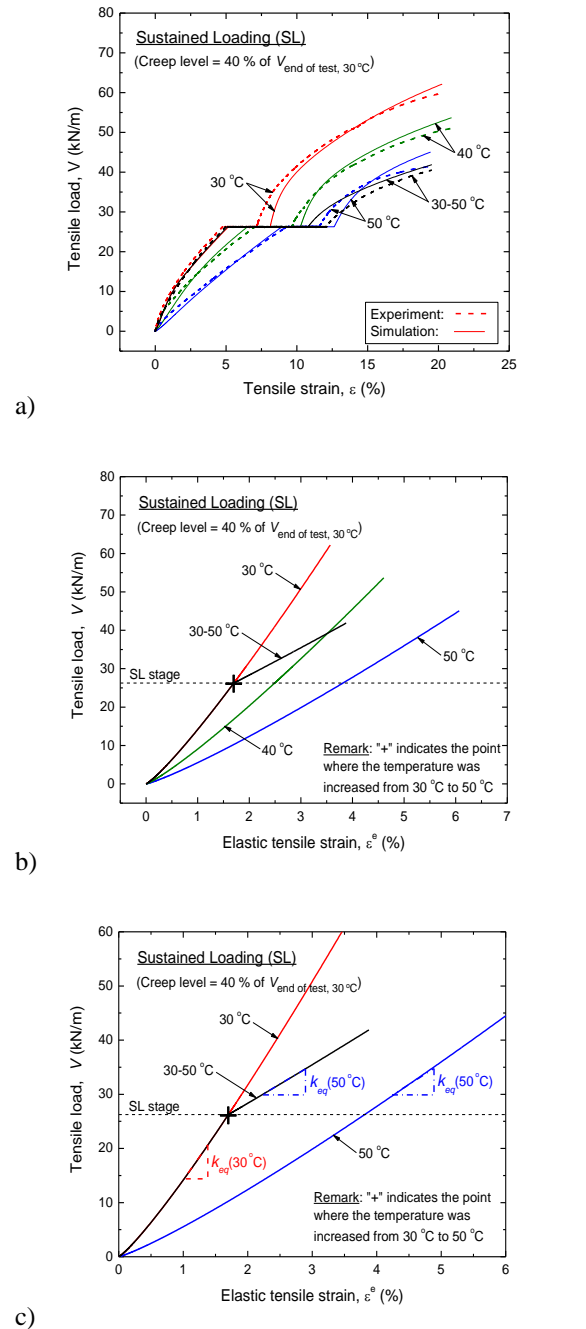


Fig. 8 Behaviours in continuous ML tests with intermediate SL under different temperatures: (a) measured and simulated  $V - \epsilon$  relations; (b) simulated  $V - \epsilon^e$  relations; and (c) zoom-up of Fig. 8(b)

- [8] Stępień S & Szymański A, "Influence of strain rate on tensile strength of woven geotextile in the selected range of temperature", *Studia Geotechnica et Mechanica*, Vol. 37, No. 2, Dec. 2015, pp. 57-60.

- [9] Chantachot T, Kongkitkul W, & Tatsuoka F “Load-strain-time behaviours of two polymer geogrids affected by temperature”, *International Journal of GEOMATE*, Vol.10, No.21, May 2016, pp. 1869-1876.
- [10] Hirakawa D, Kongkitkul W, Tatsuoka F, and Uchimura T, “Time-dependent stress-strain behaviour due to viscous properties of geogrid reinforcement”, *Geosynthetics International*, Vol. 10, No. 6, Dec. 2003, pp. 176-199.
- [11] Kongkitkul W, Chantachot T, & Tatsuoka F. “Simulation of geosynthetic load-strain-time behaviour by the non-linear three-component model”, *Geosynthetics International*, Vol.21, No.4, Aug. 2014, pp. 244-255.
- [12] Shi WZ, Peng FL, & Kongkitkul W “FE simulation of rate-dependent behaviours of polymer geosynthetic reinforcements for an estimation of mobilized tensile force in a reinforced soil”, *Computers and Geotechnics*, Vol.80, Dec. 2016, pp. 49-58.
- [13] Kongkitkul W & Tatsuoka F, “A theoretical framework to analyse the behaviour of polymer geosynthetic reinforcement in temperature-accelerated creep tests”, *Geosynthetics International*, Vol. 14, Vol. 1, Feb. 2007, pp. 23-38.

---

Copyright © Int. J. of GEOMATE. All rights reserved, including the making of copies unless permission is obtained from the copyright proprietors.

---